Optik - International Journal for Light and Electron Optics 224 (2020) 165474

Contents lists available at ScienceDirect

Optik

journal homepage: www.elsevier.com/locate/ijleo

Original research article

Research on Degree of Freedom of Secondary Mirror Truss Mechanism Based on Screw Theory and Geometry Algebra Applied on Large Telescopes

Rui Wang [a,b], Fuguo Wang [a,*], Liang Hao [a], Yuyan Cao [a], Xueqian Sun [a,b]

[a] Changchun Institute of Optics, Fine Mechanics and Physics, Chinese Academy of Sciences, Changchun, 130033, China
[b] University of Chinese Academy of Sciences, Beijing 100049, China

ARTICLE INFO

Keywords:
truss mechanism of secondary mirror
wavefront aberration
screw theory
geometric algebra

ABSTRACT

A design for a truss mechanism of a secondary mirror based on robotics is proposed. This design would allow for the construction of larger vehicle-mobile telescopes. As the new truss mechanism combines the original support structure and adjustment mechanism, the problems in designing new structures needs to be overcome. In this paper, the basic form of the truss mechanism is determined by finite element method, and the number of limbs meeting the requirements of resonance frequencies and stiffness is obtained. Degrees-of-freedom of the new truss mechanism is calculated by motion space based on geometry algebra and screw theory, It can provide more accurate and specific results compared with the G-K formula. The optimal structure is calculated to meet the requirement in degrees-of-freedom with the minimum possible limbs and kinematic pairs. After the form and the value of joints are determined, the deformations are calculated by stiffness evaluation index. Wavefront aberrations simulated with Zernike polynomials are used to verify the structure.

1. Introduction

Telescopes can either be fixed stationary or movable. Vehicle-mobile telescopes have a great advantage over ground-based telescopes in terms of mobility and efficiency. However, it is not possible to transport large telescopes by road as they do not meet height requirements of bridges and culverts. Therefore, vehicle-mobile telescopes remain in the scale of 1 m, which restricts the development of their diameter.

Secondary mirrors are generally fixed to the telescope by Serrurier truss as the supporting component and a secondary mirror assembly is installed above the Serrurier truss via Stewart platform, which adjusts the position of the mirror in six-dimensional motion [1–3]. In this type of structure, the Serrurier truss accounts for about half of the total height of the telescope, which is the main reason for over height of vehicle telescopes. As the telescope is not operated during transportation, the secondary mirror does not have to remain in the working position.

This paper presents the concept of truss mechanism in the form of robotic arms, which integrates the supporting part of traditional Serrurier truss and the adjusting part of the Stewart platform. The new designed truss has both positioning and freedom adjustment functions; thus it is necessary for the platform to have the 5 degrees-of-freedom (DOFs) except the rotation along z-axis to adjust the

* Corresponding author.
E-mail address: wfg109@163.com (F. Wang).

https://doi.org/10.1016/j.ijleo.2020.165474
Received 24 May 2020; Accepted 19 August 2020
Available online 24 August 2020

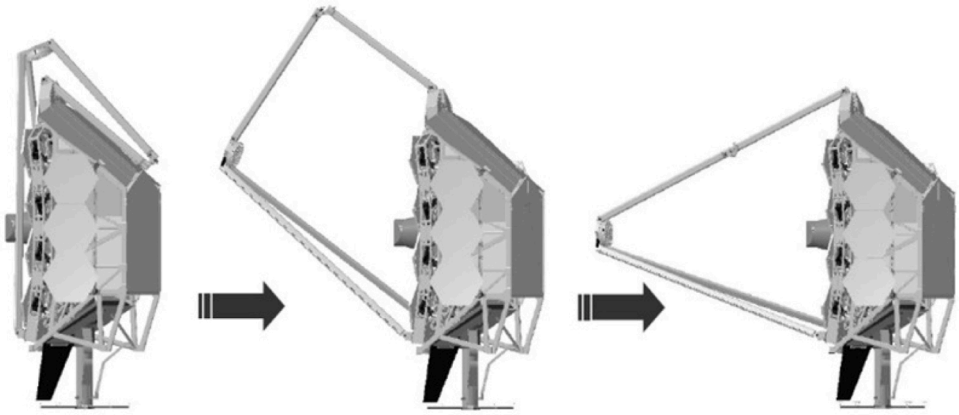

Fig. 1. view of JWST truss mechanism's expansion.

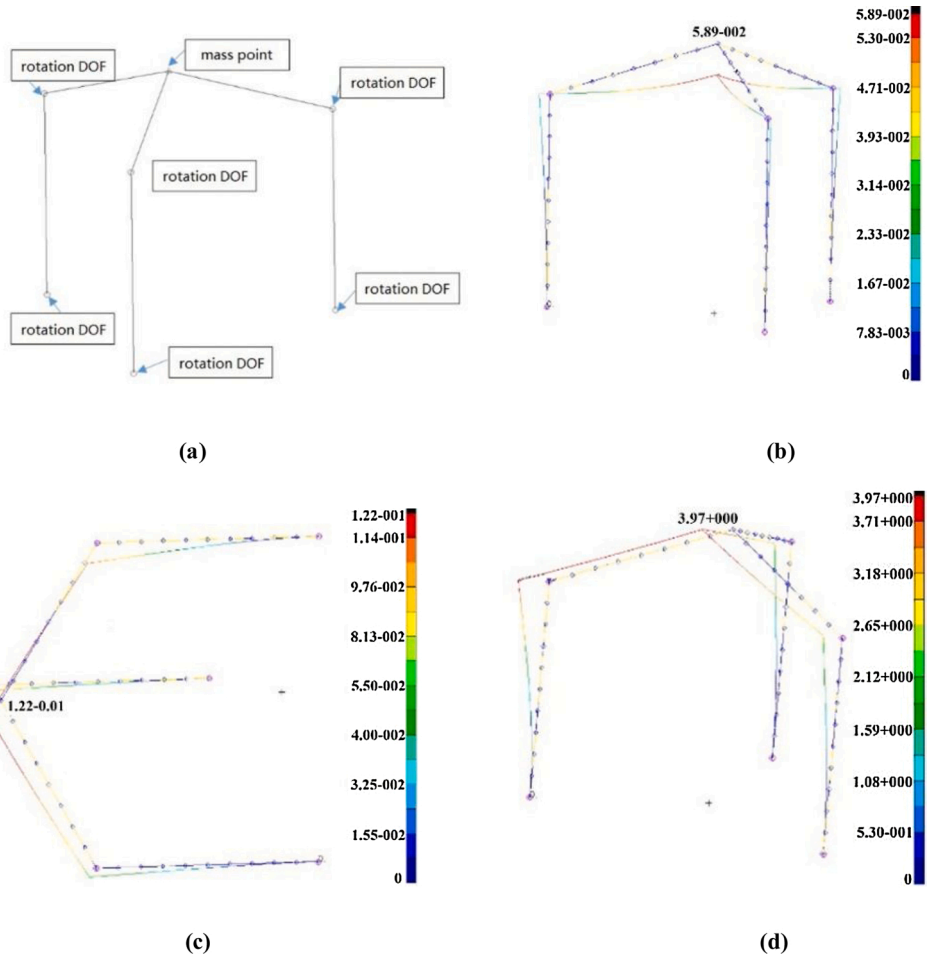

Fig. 2. finite element model of truss. **(a)** mechanical arm finite element models; **(b)** Deformation of gravity parallel to the optical axis;**(c)** Deformation of gravity vertical to the optical axis; **(d)** First-order resonant frequency cloud.

position of the secondary mirror. When the telescope is in operation, the secondary mirror assembly is placed at the specified position by the motion of the truss. When the telescope is not in operation or being transported, the secondary mirror assembly moves with the motion of the robotic arm, and the truss is placed on the side of the telescope. The height of the telescope can be reduced by half, so the overall height of the telescope is only considered from the azimuth and horizontal axis. For example, for a telescope at the scale of 2 m,

Table 1
Deformation and resonant frequency of the secondary mirror.

Deformation of gravity parallel to the optical axis	Deformation of gravity vertical to the optical axis	Resonant frequency
0.059 mm	0.12 mm	45.4 Hz

the overall height can be controlled to 4.2 m including the vehicle, so that it can be transported. The resolution and light collection capabilities of the 2 m diameter telescope increases more exponentially than the 1 m diameter telescope. The newly designed truss takes into account the image quality and mobility of the telescope, and the design has broad application prospects [4–6].

The truss mechanism based on the robotic arm cannot be constructed, because the accuracy of robotics did not meet the requirements. With advancements in technology, the accuracy has been improved. The IRB120's accuracy of ABB based on truemove and quickmove controlling software can reach 0.01 mm, which meets telescope requirements [7]. However, the robotic arm used as a truss mechanism in telescopes is very rare. A similar structure was used in the James Webber Space Telescope(JWST). The truss is folded in rocket when it is launched, and opens up when it is on track. (Fig. 1) The foldable mechanism only has 3 DOFs of rotation. Highly accuracy positioning can be achieved but it does not have the adjustment function [8–11]. The truss integrated with positioning and adjusting functions has not appeared yet.

The new truss mechanism has the function of the 6-DOFs platform. That is to say, the new robotic arm truss mechanism not only needs to meet the function of positioning the secondary mirror, but also have the 6-DOFs adjustment function. So it is necessary to calculate the number of DOF of the manipulator theoretically and design the appropriate number of limbs to take account of the stiffness and weight of the parallel mechanism. DOF of each limb and the motion subspace of the parallel structure should be optimized after meeting the freedom requirements of the secondary mirror.

2. Mechanical formulation

The truss mechanism is a key component of the telescope's structure. It's dimensional accuracy and stability directly affect the positioning accuracy of the secondary mirror. The truss mechanism produces different degrees of deflection at different positions in gravity. The telescope system needs to have sufficient stability against wind load and other problems during observation. All this indicates that the secondary mirror assembly and truss structure need to have sufficient structure stiffness [12–15].

Parallel mechanisms can lead to higher system resonant frequency and stiffness, which makes the truss a greater mass. Therefore, parameters and the number of limbs of the truss need to be adjusted to meet the stiffness of the system and limited quality requirements. In order to achieve rigidity requirement with minimum quality, structures using one limb or two limbs cannot meet the resonant frequency and the system stiffness requirements. Using three parallel limbs meets the requirements with minimum quality.

The finite element model was established to calculate the characteristics of the system. The secondary mirror is simplified as a mass point, and the mass point is set to 30 kg. Truss mechanisms are simulated as beam units and released by the corresponding rotation DOF as shown in Fig. 2(a). By establishing the finite element model shown in Fig. 2(a), gravity parallel and vertical to the optical axis is applied to the model, and the deformation and resonant frequency is verified as shown in Table 1.

The results show that the deformation of gravity parallel to the optical axis is 0.059 mm when the gravity is parallel to the optical axis as shown in Fig. 2(b). The deformation of gravity vertical to the optical axis is 0.12 mm when the gravity is parallel to the optical axis as shown in Fig. 2(c). The first order resonance is 45.4 Hz. (Fig. 2(d))

3. kinematic pair design of the truss and DOF calculation in parallel

After the theoretical analysis and verification of the finite element model, the truss mechanism is determined in the form of three parallel limbs. In order to obtain the DOF of the parallel structure, the paper designed the DOF in parallel to meet adjustment requirements by designing the type and number of DOFs of each limb based on screw theory and geometric algebra. The secondary mirror needs to have 5 DOFs except the z-axis rotation to achieve the adjustment function. The DOF of the truss mechanism is changed and compared with the requirements to obtain the optimal solution by adjusting the number of kinematic pairs on each limb.

3.1. Definitions

3.1.1. Geometric algebra and algorithm

Geometric algebra was proposed by Clifford: In real number field R, an n-dimensional vector space is recorded as V_n. Geometric algebra field $G_n = G(V_n)$ is a vector space composed of geometric products V_n space [17,18].

N-dimensional geometric algebra space G_n is composed of orthogonal groups $\{e_1, e_2, ..., e_n\}$; however, the base vectors are only algebra elements in G_n, and not basis algebra elements[19]. The basis algebra element of geometric algebra is blade. A k-blade is made up of the composition of the outer product by k(k < n) vectors $a_1, a_2, ..., a_k$:

$$\langle A_k \rangle = a_1 \wedge a_2 \wedge ... \wedge a_k \tag{1}$$

where k is the order of the blade; therefore $\langle A \rangle_k$ is also known as the k-order blade. $\langle A \rangle_k$ represents a directional subspace formed by

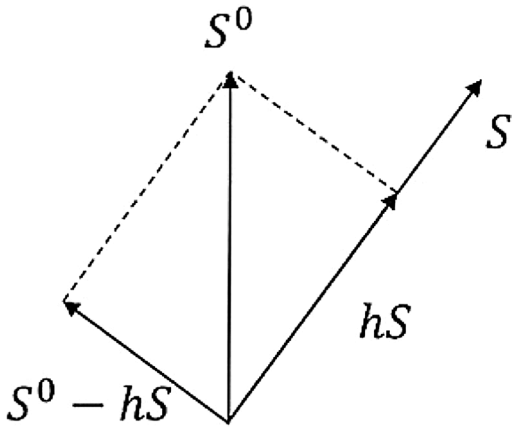

Fig. 3. axis of screw.

these k-vectors. In particular, when k = 0, $\langle A\rangle_0$ represents a scalar, when k = 1, $\langle A\rangle_1$ represents a vector [20–22]. N-dimensional geometric algebra G_n is composed of 0-n order blade.

The geometric product is a unique algorithm of geometric algebra and defined as *ab*, which is composed of the sum of the inner and outer products of vectors *a* and *b*.

$$ab = a \cdot b + a \wedge b \tag{2}$$

$a \cdot b$ is the inner product of *a* and *b*, $a \wedge b$ is the outer product of *a* and *b*.

3.1.2. Relationship establishment between screw theory and geometric algebra

According to the definition of the screw theory [23,24], a screw may represent the motion and force of a rigid body, which is the speed or the force of the rigid body. Screw is a line vector with a pitch, and the equation of the screw is $r \times S = S^0 - hS$ (Fig. 3), written in Plücker coordinates as $(S; S^0 - hS)$.

A screw can thus be expressed as:

$$\begin{array}{l} \$ = \left(S; S^0\right) \\ = \left(S; S^0 - hs\right) + (0; hS) \\ (s; r \times s + hs) \\ (l, m, n; p, q, r) \end{array} \tag{3}$$

r represents a position vector of a point on a line, *h* represents a pitch, l, m, n, p, q, r are set as the Plücker coordinates of the screw. Contact is established between screw theory and algebraic geometry to solve for the degrees of freedom. The screw *S* can be written as

$$\begin{array}{l} S = s + r \wedge s + hi_3 s \\ = v_1 e_1 + v_2 e_2 + v_3 e_3 + (v_3 y - v_2 z) e_2 \wedge e_3 + (v_1 z - v_3 x) e_3 \wedge e_1 \\ + (v_2 x - v_1 y) e_1 \wedge e_2 + h v_1 e_2 \wedge e_3 + h v_2 e_3 \wedge e_1 + h v_3 e_1 \wedge e_2 \\ = v_1 e_1 + v_2 e_2 + v_3 e_3 + b_1 e_2 \wedge e_3 + b_2 e_3 \wedge e_1 + b_3 e_1 \wedge e_2 \end{array} \tag{4}$$

b_i is a scalar, $b_1 = v_3 y - v_2 z + h v_1$, $b_2 = v_1 y - v_3 z + h v_2$, $b_3 = v_2 y - v_1 z + h v_3$. The method is extended from the three-dimensional representation to R(6 0) geometric algebraic space, R(6 0) is a six-dimensional geometric algebra space, $e_1, e_2, e_3, e_4, e_5, e_6$ is a set of orthogonal base units of R^6, and set

$$\begin{array}{c} e_4 = e_2 \wedge e_3, e_5 = e_3 \wedge e_1, e_6 = e_1 \wedge e_2 \\ e_1^2 = e_2^2 = e_3^2 = e_4^2 = e_5^2 = e_6^2 = 1, e_i e_j = -e_j e_i (i \neq j) \end{array}, \tag{5}$$

The screw can then be represented by geometric algebra as:

$$S = v_1 e_1 + v_2 e_2 + v_3 e_3 + b_1 e_4 + b_2 e_5 + b_3 e_6 \tag{6}$$

3.2. DOF design of the truss mechanism limb

It is difficult to obtain symbols or analytical expressions when solving the DOF problem using the modified G-K formula [12]. In this paper, the screw theory combined with geometric algebra is used to obtain the motion subspace on the moving platform by the union of the twists on the limbs.

The optimal process to meet the requirement of secondary mirror adjustment with few joints is shown in Fig. 4.

Step 1, set the initial kinematic pair type and the number *n*.

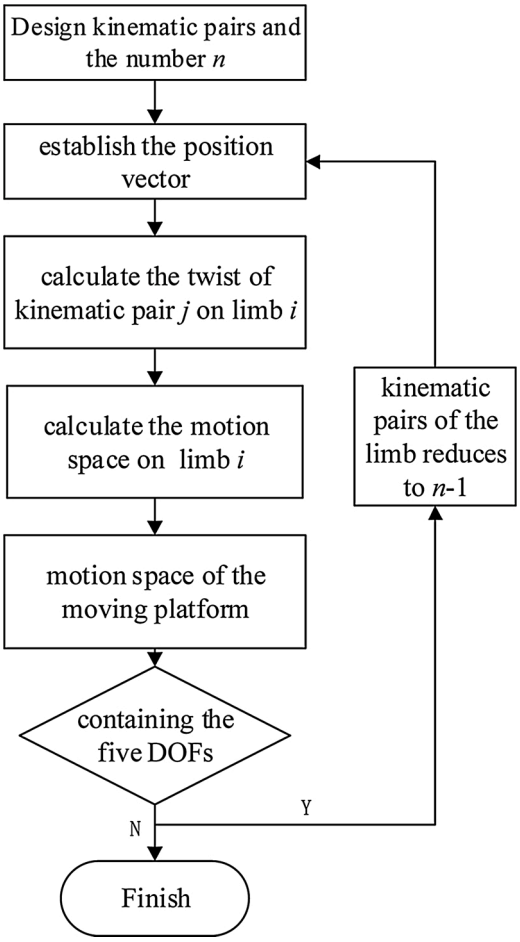

Fig. 4. process of limb kinematic pair design.

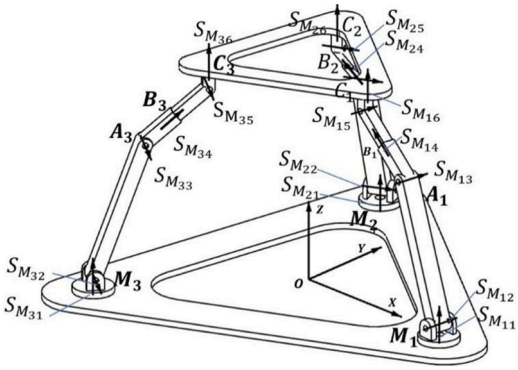

Fig. 5. Structure of parallel truss mechanism.

Step 2, establish the position vector of each kinematic pair.

Step 3, calculate each twist on each limb.

Step 4, calculate the motion space of the end of each limb.

Step 5, solve the motion space of the moving platform, verify whether the moving platform contains the five DOFs in addition to the rotation along z-axis. If the kinematics meets the requirements, the kinematic pair of the limb is reduced to *n-1*. If the kinematics do not meet the requirements, the kinematic pair of the last loop is the optimal solution.

As secondary mirror adjustment mechanism needs to be isotropic for adjustment, symmetrical parallel mechanism is used in this

Table 2
Position vector and twist in a fixed coordinate system.

position vector	coordinates	twist
OM_1	$[r,0,0]$	$S_{M_{11}}, S_{M_{12}}$
OM_2	$[-\frac{1}{2}r, \frac{\sqrt{3}}{2}r, 0]$	$S_{M_{21}}, S_{M_{22}}$
OM_3	$[-\frac{1}{2}r, -\frac{\sqrt{3}}{2}r, 0]$	$S_{M_{31}}, S_{M_{32}}$
OA_1	$[x_{A_1}, y_{A_1}, z_{A_1}]$	$S_{M_{13}}$
OA_2	$[x_{A_2}, y_{A_2}, z_{A_2}]$	$S_{M_{23}}$
OA_3	$[x_{A_3}, y_{A_3}, z_{A_3}]$	$S_{M_{33}}$
OB_1	$[x_{B_1}, y_{B_1}, z_{B_1}]$	$S_{M_{14}}$
OB_2	$[x_{B_2}, y_{B_2}, z_{B_2}]$	$S_{M_{24}}$
OB_3	$[x_{B_3}, y_{B_3}, z_{B_3}]$	$S_{M_{34}}$
OC_1	$[x_{C_1}, y_{C_1}, z_{C_1}]$	$S_{M_{15}}, S_{M_{16}}$
OC_2	$[x_{C_2}, y_{C_2}, z_{C_2}]$	$S_{M_{25}}, S_{M_{26}}$
OC_3	$[x_{C_3}, y_{C_3}, z_{C_3}]$	$S_{M_{35}}, S_{M_{36}}$

study. Three limbs of truss are circumferentially distributed on the four-way body, the beginning and the end of the robotic arms seem to be equilateral triangles. The forms of the kinematic pairs are generally revolute pair R, prismatic pair P, spherical pair S. To reduce the overall weight of the truss structure, torque motors are used in this structure, thus revolute pairs are used. The R pair can provide one relative DOF. In this paper, the initial value is set to 6; thus, the initial DOF of each limb is 6. Establishment of the coordinate system is shown in Fig. 5, where the origin is at the center of the fixed platform plane.

Radius of the platform is set to r, and the coordinate points $A_1, A_2, A_3, B_1, B_2, B_3, C_1, C_2$, and C_3 are set as shown in Table 2. Point M_1 is provided with two revolute pairs, the axes of screw are parallel to the z-axis and y-axis. A_1 is provided with one revolute pair, the axis of the screw is parallel to the y-axis ; B_1 is provided with one revolute pair, the axis of the screw is located in the xz plane; C_1 is provided with two revolute pairs, the axes of screw are parallel to the z-axis and y-axis. The screw system of the other two limbs can be obtained from rotation about the z-axis.

According to Eq. (6), each twist on the first limb can be written as:

$$\begin{aligned}
S_{M_{11}} &= e_3 \\
S_{M_{12}} &= e_2 + re_6 \\
S_{M_{13}} &= e_2 - z_{A_1}e_4 + x_{A_1}e_6 \\
S_{M_{14}} &= e_1 + z_{B_1}e_4 - y_{B_1}e_6 \\
S_{M_{15}} &= e_2 - z_{C_1}e_4 + x_{C_1}e_6 \\
S_{M_{16}} &= e_3 + y_{C_1}e_4 - x_{C_1}e_6
\end{aligned} \tag{7}$$

The motion subspace of the first limb can be regarded as series of independent kinematic pairs on the limb, then the union of the twists is:

$$\begin{aligned}
S_{M_1} &= S_{M_{11}} \cup S_{M_{12}} \cup S_{M_{13}} \cup S_{M_{14}} \cup S_{M_{15}} \cup S_{M_{16}} \\
&= S_{M_{11}} \wedge S_{M_{12}} \wedge S_{M_{13}} \wedge S_{M_{14}} \wedge S_{M_{15}} \wedge S_{M_{16}} \\
&= ae_1 \wedge e_2 \wedge e_3 \wedge e_4 \wedge e_5 \wedge e_6
\end{aligned} \tag{8}$$

Among them, a is a scalar, $a = x_{C_1}(y_{A_1} - rz_{C_1} - z_{A_1}y_{C_1} + rz_{A_1})$. Eq. (8) represents the motion subspace at the end of the kinematic chain on the first limb is a 6-blade. Similarly, according to Eq. (8), each twist on the second limb can be written as:

$$\begin{aligned}
S_{M_{21}} &= e_3 \\
S_{M_{22}} &= \frac{\sqrt{3}}{2}e_1 + \frac{1}{2}e_2 - re_6 \\
S_{M_{23}} &= \frac{\sqrt{3}}{2}e_1 + \frac{1}{2}e_2 - \frac{1}{2}z_{A_2}e_4 + \frac{\sqrt{3}}{2}z_{A_2}e_5 - x_{A_2}e_6 \\
S_{M_{24}} &= -\frac{1}{2}e_1 + \frac{\sqrt{3}}{2}e_2 + \frac{1}{2}z_{B_2}e_5 + \frac{\sqrt{3}}{2}z_{B_2}e_4 - y_{B_2}e_6 \\
S_{M_{25}} &= \frac{\sqrt{3}}{2}e_1 + \frac{1}{2}e_2 - \frac{1}{2}z_{C_2}e_4 + \frac{\sqrt{3}}{2}z_{C_2}e_5 - x_{C_2}e_6 \\
S_{M_{26}} &= e_3 + y_{C_2}e_4 - x_{C_2}e_5
\end{aligned} \tag{9}$$

The motion subspace of the second limb is the union of the twists:

$$\begin{aligned}
S_{M_2} &= S_{M_{21}} \cup S_{M_{22}} \cup S_{M_{23}} \cup S_{M_{24}} \cup S_{M_{25}} \cup S_{M_{26}} \\
&= S_{M_{21}} \wedge S_{M_{22}} \wedge S_{M_{23}} \wedge S_{M_{24}} \wedge S_{M_{25}} \wedge S_{M_{26}} \\
&= be_1 \wedge e_2 \wedge e_3 \wedge e_4 \wedge e_5 \wedge e_6
\end{aligned} \tag{10}$$

among them, b is a scalar,

$$
\begin{aligned}
b = {} & y_{C_2}(\frac{\sqrt{3}}{2}z_{A_2}x_{C_2} - \frac{1}{2}(\frac{3}{4}z_{A_2}y_{B_2} - \frac{3}{4}x_{A_2}z_{B_2} + \frac{\sqrt{3}}{4}rz_{B_2} + \frac{\sqrt{3}}{4}rz_{A_2}) \\
& - \frac{\sqrt{3}}{2}z_{C_2}(x_{A_2} - r) + \frac{\sqrt{3}}{2}(\frac{\sqrt{3}}{4}z_{A_2}y_{B_2} - \frac{1}{4}x_{A_2}z_{B_2} + \frac{1}{4}rz_{B_2} - \frac{3}{4}rz_{A_2})) \\
& + x_{C_2}(-\frac{1}{2}x_{C_2} - \frac{1}{2}(\frac{\sqrt{3}}{4}z_{A_2}y_{B_2} - \frac{3}{4}x_{A_2}z_{B_2} + \frac{3}{4}r - \frac{1}{4}rz_{A_2}) + \frac{1}{2}z_{C_2}(x_{A_2} - r) \\
& + \frac{\sqrt{3}}{2}(-\frac{1}{4}z_{A_2}y_{B_2} - \frac{\sqrt{3}}{4}x_{A_2}z_{B_2} + \frac{\sqrt{3}}{4}rz_{B_2} + z_{A_2}))
\end{aligned}
$$

Each twist on the third limb can be written as:

$$
\begin{aligned}
S_{M_{31}} &= e_3 \\
S_{M_{32}} &= \frac{\sqrt{3}}{2}e_1 - \frac{1}{2}e_2 + re_6 \\
S_{M_{33}} &= \frac{\sqrt{3}}{2}e_1 - \frac{1}{2}e_2 + \frac{1}{2}z_{A_3}e_4 + \frac{\sqrt{3}}{2}z_{A_3}e_5 - x_{A_3}e_6 \\
S_{M_{34}} &= \frac{1}{2}e_1 + \frac{\sqrt{3}}{2}e_2 - \frac{1}{2}z_{B_3}e_5 + \frac{\sqrt{3}}{2}z_{B_3}e_4 - y_{B_3}e_6 \\
S_{M_{35}} &= \frac{\sqrt{3}}{2}e_1 - \frac{1}{2}e_2 + \frac{1}{2}z_{C_3}e_4 + \frac{\sqrt{3}}{2}z_{C_3}e_5 - x_{C_3}e_6 \\
S_{M_{36}} &= e_3 + y_{C_2}e_4 - x_{C_2}e_5
\end{aligned}
\tag{11}
$$

The motion subspace of the third limb is the union of the twists:

$$
\begin{aligned}
& S_{M_3} = S_{M_{31}} \cup S_{M_{32}} \cup S_{M_{33}} \cup S_{M_{34}} \cup S_{M_{35}} \cup S_{M_{36}} \\
& = S_{M_{31}} \wedge S_{M_{32}} \wedge S_{M_{33}} \wedge S_{M_{34}} \wedge S_{M_{35}} \wedge S_{M_{36}} \\
& = ce_1 \wedge e_2 \wedge e_3 \wedge e_4 \wedge e_5 \wedge e_6
\end{aligned}
\tag{12}
$$

among them, c is a scalar.

$$
\begin{aligned}
c = {} & y_{C_3}(\frac{\sqrt{3}}{2}z_{A_3}x_{C_3} + \frac{1}{2}(\frac{3}{4}z_{A_3}y_{B_3} + \frac{3}{4}x_{A_3}z_{B_3} + \frac{\sqrt{3}}{4}rz_{B_3} + \frac{\sqrt{3}}{4}rz_{A_3}) \\
& - \frac{\sqrt{3}}{2}z_{C_3}(x_{A_3} - \frac{1}{2}r) + \frac{\sqrt{3}}{2}(-\frac{\sqrt{3}}{4}z_{A_3}y_{B_3} - \frac{1}{4}x_{A_3}z_{B_3} - \frac{1}{4}rz_{B_3} + \frac{3}{4}rz_{A_3})) \\
& + x_{C_3}(\frac{1}{2}x_{C_3} + \frac{1}{2}(\frac{\sqrt{3}}{4}z_{A_3}y_{B_3} - \frac{3}{4}x_{A_3}z_{B_3} - \frac{3}{4}r + \frac{1}{4}rz_{A_3}) - \frac{1}{2}z_{C_3}(x_{A_3} - \frac{1}{2}r) \\
& + \frac{\sqrt{3}}{2}(-\frac{1}{4}z_{A_3}y_{B_3} + \frac{\sqrt{3}}{4}x_{A_3}z_{B_3} + \frac{\sqrt{3}}{4}rz_{B_3} + z_{A_3}))
\end{aligned}
$$

n-dimensional geometric algebra G_n comprises a 0-n order blade, wherein the blade of 0 order is a scalar. It is then easy to obtain the following equation:

$$
\begin{aligned}
& S_M = S_{M_1} \cap S_{M_2} \cap S_{M_3} \\
& = me_1 \wedge e_2 \wedge e_3 \wedge e_4 \wedge e_5 \wedge e_6
\end{aligned}
\tag{13}
$$

m can be calculated by Eqs. (8),(10),(12), and m is a scalar that does not influence the result. Therefore, if the DOF of each limb is 6, the DOF in parallel is 6 with 3DOFs of translation and 3DOFs of rotation. Thus the mechanism meets the requirement of secondary mirror adjustment.

Because it is not necessary to have rotation DOF along the z-axis, in order to minimize the number of kinematic pair and obtain an optimal solution, the z-axis rotation freedom in three limbs is removed, which is the revolute pair parallel to the z-axis in C_1, C_2, and C_3 in Fig.5. The primary mechanism is changed to 3-RRRRR parallel mechanism and DOF is calculated again.

According to the data in Table 2, the motion subspace of the first limb is the union of the twists:

$$
\begin{aligned}
& S_{M_1} = S_{M_{11}} \cup S_{M_{12}} \cup S_{M_{13}} \cup S_{M_{14}} \cup S_{M_{15}} \\
& = S_{M_{11}} \wedge S_{M_{12}} \wedge S_{M_{13}} \wedge S_{M_{14}} \wedge S_{M_{15}} \\
& = a_1e_1 \wedge e_2 \wedge e_3 \wedge e_4 \wedge e_6 + a_2e_2 \wedge e_3 \wedge e_4 \wedge e_5 \wedge e_6
\end{aligned}
\tag{14}
$$

Among them, a_1, a_2 are scalar.

The motion subspace of the second limb is the union of the twists:

$$\begin{aligned} S_{M_2} &= S_{M_{21}} \cup S_{M_{22}} \cup S_{M_{23}} \cup S_{M_{24}} \cup S_{M_{25}} \\ &= S_{M_{21}} \wedge S_{M_{22}} \wedge S_{M_{23}} \wedge S_{M_{24}} \wedge S_{M_{25}} \\ &= e_1 \wedge e_2 \wedge e_3 \wedge e_4 \wedge e_5 + b_1 e_1 \wedge e_2 \wedge e_3 \wedge e_4 \wedge e_6 + b_2 e_1 \wedge e_3 \wedge e_4 \wedge e_5 \wedge e_6 \\ &+ b_3 e_1 \wedge e_2 \wedge e_3 \wedge e_5 \wedge e_6 + b_4 e_2 \wedge e_3 \wedge e_4 \wedge e_5 \wedge e_6 \end{aligned} \tag{15}$$

Among them, b_1, b_2, b_3, b_4 are scalar.

The motion subspace of the third limb is the union of the twists:

$$\begin{aligned} S_{M_3} &= S_{M_{31}} \cup S_{M_{32}} \cup S_{M_{33}} \cup S_{M_{34}} \cup S_{M_{35}} \\ &= S_{M_{31}} \wedge S_{M_{32}} \wedge S_{M_{33}} \wedge S_{M_{34}} \wedge S_{M_{35}} \\ &= e_1 \wedge e_2 \wedge e_3 \wedge e_4 \wedge e_5 + c_1 e_1 \wedge e_2 \wedge e_3 \wedge e_4 \wedge e_6 + c_2 e_1 \wedge e_3 \wedge e_4 \wedge e_5 \wedge e_6 \\ &+ c_3 e_1 \wedge e_2 \wedge e_3 \wedge e_5 \wedge e_6 + c_4 e_2 \wedge e_3 \wedge e_4 \wedge e_5 \wedge e_6 \end{aligned} \tag{16}$$

Among them, c_1, c_2, c_3, c_4 are scalar.

The union of twists on the 3 limbs is 5-blades from the observations of Eqs. (14),(15),(16).

$$\begin{aligned} S_M &= S_{M_1} \cap S_{M_2} \cap S_{M_3} \\ &= \left((S_{M_1} \cap S_{M_2}) I_6^{-1} \right) \cap S_{M_3} \\ &= a_{10} e_1 \wedge e_3 \wedge e_4 + a_{20} e_1 \wedge e_2 \wedge e_3 + a_{30} e_2 \wedge e_3 \wedge e_4 \end{aligned} \tag{17}$$

Decompose the equation according to the blade decomposition method

$$\begin{aligned} S_1 &= \frac{1}{a_{30}} (a_{20} e_1 + e_4) \\ S_2 &= \frac{1}{a_{30}} (a_{10} e_1 + e_2) \\ S_3 &= e_3 \end{aligned} \tag{18}$$

Among them, a_{10}, a_{20}, a_{30} are scalar, which has no impact on the results and can be obtained according to equations (16),(17), and (18).

In Eq. (20), 3-RRRRR is shown as a 3-blade, and its motion subspace comprises S_1, S_2, and S_3. Therefore, this parallel mechanism of 3-RRRRR has 3DOFs. S_1 indicates that the Plücker coordinates of the screw are (a_{20} 1 0 ; 0 0 0), the pitch is $1/a_{20}$; S_2 is a DOF of rotation and the Plücker coordinates is (a_{20} 1 0 ; 0 0 0); S_3 indicates a DOF of translation along the z-axis. The calculation result shows that 3-RRRRR does not meet the DOF of secondary mirror requirement. The 3-6R in Eq. (15) has 6-DOFs in motion subspace and meets the requirement of the secondary mirror adjustment, thus the 3-6R is the optimal solution.

4. Verification

Although stiffness and resonance frequencies are simulated in Section 2, the value and the position of joints has changed after the DOF calculation in Section 3, the stiffness of the truss changes as well. So stiffness evaluation index is used to verify the stiffness in this paper. The truss system is simulated with gravities along different orientations in matlab. Rotation and translation deformations are used to analysis wavefront aberrations. The result is compared with system requirement to verify the performance.

4.1. Stiffness evaluation index

Because the truss is a symmetric parallel mechanism, one limb is optimized in this paper instead of the whole parallel mechanism to make the analysis easier, and the parallel stiffness matrix is calculated after the optimization. The enhanced stiffness model proposed by Ref. [16] is expressed as:

$$K = J^{-T} (K_\theta - K_C) J^{-1} \tag{19}$$

Where K_C denotes a complementary stiffness matrix. K_θ is defined as:

$$K_\theta = \begin{bmatrix} k_1 & 0 & \cdots & 0 \\ 0 & k_2 & \cdots & 0 \\ \vdots & \vdots & \ddots & \vdots \\ 0 & 0 & \cdots & k_6 \end{bmatrix} = \begin{bmatrix} K_{11} & K_{12} \\ K_{21} & K_{22} \end{bmatrix} \tag{20}$$

Where $k_i (i = 1, 2, \ldots, 6)$ is the stiffness of J_i, K_{11}, K_{12}, K_{21} and K_{22} are 3×3 submatrices of K_θ.

It can be seen that calculation of the inverse Jacobian matrix is involved from Eq. (21), which inevitably introduces a calculation error when the robot is close to singularities. To solve such problem, a compliance model derived by Ref. [25] was proposed and defined as:

$$C = J K_\theta^{-1} J^T = \begin{bmatrix} C_{tt} & C_{tr} \\ C_{tr}^T & C_{rr} \end{bmatrix} \tag{21}$$

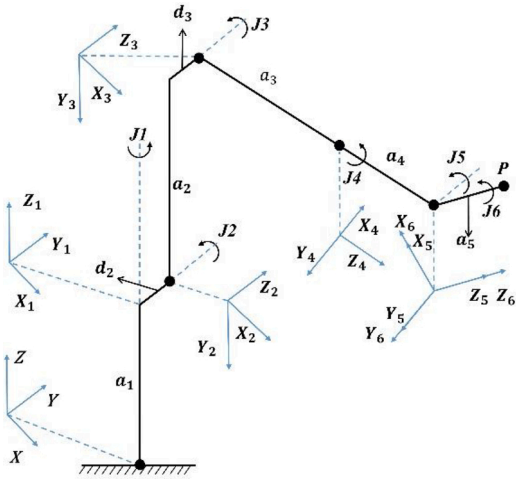

Fig. 6. DHm parameterization of the limb and the position of joints.

Table 3
DHm parameters of the limb and the position of joints.

	J1	J2	J3	J4	J5	J6
$\theta_i(rad)$	θ_1	$\theta_2 = -\frac{7\pi}{20}$	$\theta_3 = \frac{\pi}{5}$	$\theta_4 = 0$	$\theta_5 = 0$	θ_6
$\alpha_i(\mathrm{deg})$	-90°	0°	-90°	90°	-90°	α_6
$a_i(mm)$	$a_1 = 200$	$a_2 = 1700$	$a_3 = 1800$	$a_4 = 0$	$a_5 = 200$	a_6
$d_i(mm)$	0	d_2	d_3	0	0	d_6

Where C_{tt}, C_{tr} and C_{rr} are the 3×3 translational, coupling and rotational compliance submatrices, which are not the inverse of the stiffness submatrix [26].

By neglecting the toque applied to the end-effector(EE) [27], the overall compliance of the robot is proportional to the volume of the translational compliance ellipsoid. Thus, the performance index of the robot stiffness proposed by Ref. [28] can be defined as:

$$k_{stif} = \frac{1}{\sqrt[3]{\det(C_{tt})}} = \frac{1}{\sqrt[3]{\det(J_{11}K_{11}^{-1}J_{11}^{T} + J_{12}K_{22}^{-1}K_{12}^{T})}} \tag{22}$$

where J_{11} and J_{12} are 3×3 submatrices of J, which can be written as:

$$J = \begin{bmatrix} J_{11} & J_{12} \\ J_{21} & J_{22} \end{bmatrix} \tag{23}$$

The proposed methodology aims at calculating the translational deformation Δx and rotational deformation $\Delta\theta$ of the secondary mirror, which is defined as:

$$\begin{bmatrix} \Delta x \\ \Delta\theta \end{bmatrix} = \begin{bmatrix} C_{tt}f \\ C_{tr}^{T}f \end{bmatrix} = \begin{bmatrix} C_{tt} \cdot f \cdot e_f \\ C_{tr}^{T} \cdot f \cdot e_f \end{bmatrix} \tag{24}$$

Obviously, to calculate the deformation, the compliance matrix C needs to be calculated with different force direction e_f. Different e_f is used to verify the wavefront aberrations caused by gravity. As Ref. [28] described, the compliance performance index can be used to evaluate the stiffness in one position.

4.2. Wavefront Aberrations Verification by Zernike Polynomials

For a truss mechanism in 2 m scale, the joint stiffness of Smart5 NJ 220-2.7 robot is used to analysis in this paper. Then, the K_θ is identified as diag[1.5727×10^9, 6.7566×10^9, 1.1169×10^9, 3.3249×10^8, 1.1038×10^8, 4.1444×10^8]($N \cdot mm/rad$). For serial manipulators, the Jacobian matrix is established at the point P of the EE as shown in Fig. 6.

DHm parameters to calculate deformations are shown in Table 3. J6 doesn't show up in the Jacobian matrix. θ_4 is set to 0 in order to make the z-axis of primary mirror and secondary mirror is coaxial.

The 3-6R structure is composed of 3 same limbs. C_1, C_2, C_3 are compliance matrix of the EE. C_2, C_3 can be obtained through the transmission matrix.

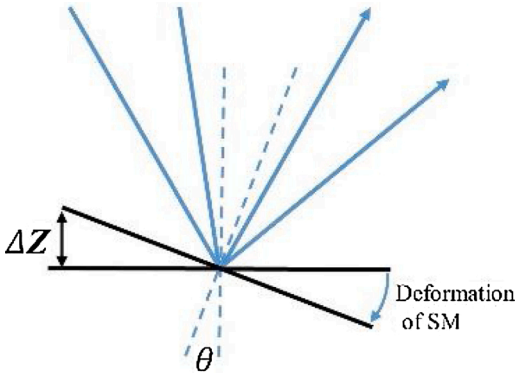

Fig. 7. ΔZ caused by tip and tilt.

Table 4
deformations and wavefront aberrations caused by gravity.

	$Z_{\max}(mm)$	$Z_{\min}(mm)$	$\Delta Z(mm)$	$LS(nm)$
$e_f = [0,0,1]^T$	1.49856e-3	1.49719e-3	1.37234e-6	2.74467
$e_f = [1,0,0]^T$	3.56316e-4	3.55540e-4	7.76540e-7	1.55308

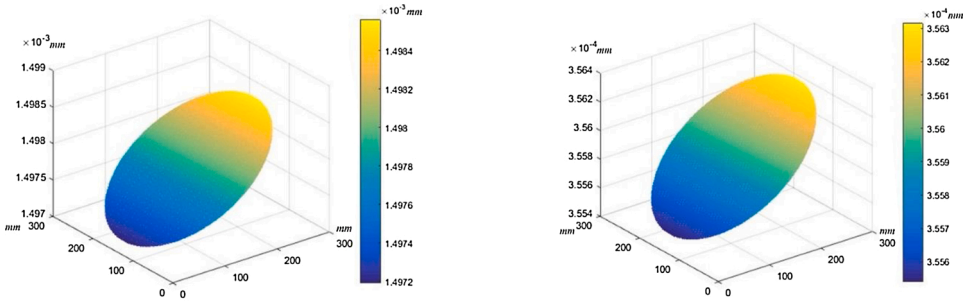

(a) (b)

Fig. 8. Aberrations caused by deformations in gravity**(a)** gravity parallel to the z-axis**(b)** gravity parallel to the x-axis.

$$C_2 = T_{\frac{2\pi}{3}} \cdot C_1 \cdot T_{\frac{2\pi}{3}}^T \tag{25}$$

$$C_3 = T_{\frac{4\pi}{3}} . C_1 . T_{\frac{4\pi}{3}}^T \tag{26}$$

Thus, the parallel flexibility matrix of the structure is

$$C_{tt} = (C_{tt1}^{-1} + C_{tt2}^{-1} + C_{tt3}^{-1})^{-1} \tag{27}$$

$$C_{tr} = (C_{tr1}^{-1} + C_{tr2}^{-1} + C_{tr3}^{-1})^{-1} \tag{28}$$

Then, C_{tt} and C_{tr} is obtained.

$$C_{tt} = \begin{bmatrix} 2.62003e\text{-}4 & 9.851853e\text{-}5 & 3.55928e\text{-}4 \\ 9.85185e\text{-}5 & 1.78827e\text{-}3 & -7.15779e\text{-}5 \\ 3.55928e\text{-}4 & -7.15779e\text{-}5 & 1.49788e\text{-}3 \end{bmatrix} \quad C_{tr} = \begin{bmatrix} 2.01576e\text{-}8 & -1.93230e\text{-}7 & 2.77446e\text{-}8 \\ 3.88870e\text{-}7 & 0 & 6.88193e\text{-}7 \\ -1.46454e\text{-}8 & -1.29434e\text{-}6 & -2.01576e\text{-}8 \end{bmatrix}$$

After the compliance matrix is obtained, deformation of the secondary mirror in different gravities can be calculated by Eq. (26). Deformation along each direction is calculated by decomposing Δx and $\Delta\theta$. Due to analyzing the rigid body deformation, only piston, tip and tilt are considered in this paper. First three order aberrations will be obtained after the result is measured by Zernike polynomials. Finally, the value of deviation is compared with the system error requirement.

Because the value of θ caused by ΔZ is small enough in Fig. 7, $\sin\theta = \theta$. The aberration caused by ΔZ can be written as $LS = \theta \cdot f =$

$\frac{\Delta Z}{D} \cdot f$. According to the results shown in Table 4, the wavefront aberrations caused by the deformation of the secondary mirror are 2.74467 nm and 1.55308 nm under gravity along z-axis and x-axis separately. The result meets the aberration requirement, which means the design meets the requirement of the telescope system (Fig. 8).

5. Conclusion

This paper presents a concept for truss on large telescopes based on robotics. The newly designed truss mechanism combines supporting and adjusting mechanisms and makes it possible to construct larger vehicle-mobile telescopes, and also allows for the secondary mirror to be more conveniently replaced. Based on this idea, this paper obtains and verifies 3 limbs in parallel is the lightest project to meet the requirement of the system. DOF of the moving platform is calculated and obtained by varying the number of kinematic pairs in the limb based on screw theory and geometry algebra. The optimal solution is using 3 limbs and each limb has 6 kinematic pairs according to the requirements of the telescope system. The aberration caused by the secondary mirror is verified to meet the error requirement.

Author Agreement

All authors have read and approved to submit it to your journal. There is no conflict of interest of any authors in relation to the submission. This paper has not been submitted elsewhere for consideration of publication.

Declaration of Competing Interest

The authors declare that they have no conflict of interest.

Acknowledgement

This work is supported by Youth Science Foundation of the Chinese Academy of Sciences (CAS) (No. 11803035).

References

[1] W. Sutherland, J. Emerson, G. Dalton, E. Atadettedgui, S. Beard, R. Bennett, The Visible and Infrared Survey Telescope for Astronomy (VISTA): Design, technical overview, and performance, Astronomy& Astrophysics 575 (2014). A25(1)-A25(27).
[2] V. Ford, C. Carter, C. Delrez, P. Fumi, E. Gabriel, D. Gallieni, Jitter studies for the secondary and tertiary mirror systems on the Thirty Meter Telescope, SPIE Astronomical Telescopes+Instrumentation 9151 (2014), 91512H.
[3] Z. Nan, C. Li, G. Wei, Z.X. Song, Z. Chao, G.R. Ren, A secondary mirror adjustment system with hexapod structure for optical telescope application, SPIE Society of Photo-optical Instrumentation Engineers 9280 (2014), 92800N.
[4] S. Psilodimitrakopoulos, L. Mouchliadis, I. Paradisanos, A. Lemonis, G. Kioseoglou, E. Stratakis, Ultrahigh-resolution nonlinear optical imaging of the armchair orientation in 2D transition metal dichalcogenides, Light: Science & Applications 7 (2018) 1–9.
[5] R. Kammel, R. Ackermann, J. Thomas, J. Gotte, S. Skupin, A. Tunnermann, S. Nolte, Enhancing precision in fs-laser material processing by simultaneous spatial and temporal focusing, vol 3, 2014, pp. 1–8.
[6] C. Hu, J. Liu, J. Wang, Z. Gu, C. Li, Q. Li, Y. Li, S. Zhang, C. Bi, X. Fan, W. Zheng, New design for highly durable infrared-reflective coatings, vol 7, 2018, pp. 1–11.
[7] N. Albert, A.B. Ilian, Absolute calibration of an ABB IRB 1600 robot using a laser tracker, Robotics and Computer-Integrated Manufacturing 29 (2013) 236–245.
[8] C. Atkinson, S. Texter, R. Keskikuha, L. Feinberg, Status of the JWST optical telescope element, SPIE Astronomical Telescopes+Instrumentation 6265 (2006), 62650T.
[9] D. Porpora, J. Wachs, A. Barto, J.S. Knight, Mirror placement optimization for the multi-segmented James Webb Space Telescope primary mirror, SPIE Astronomical Telescopes+ Instrumentation (2014) 9143, 9143O.
[10] T. Hadjimichael, R.G. Ohl, S. Antonille, D.L. Aronstein, W. Eichhorn, Alignment of the James Webb Space Telescope Integrated Science Instrument Module Element, SPIE Optical Engineering+ Applications 9951 (2016), 99510C.
[11] M. Clampin, Recent progress with the JWST Observatory, SPIE Astronomical Telescopes+ Instrumentation 9143 (2014), 914302.
[12] L. Bin, W. Xiaoxia, L. Jianfeng, M. Ming, L. Xiangyi, Y. Hongbo, Influence of axial-force errors on the deformation of the 4m lightweight mirror and its correction, Applied Optics 56 (2017) 611–619.
[13] H.C. Zhao, J.X. Zhang, Secondary mirror supporting structure for 1.2m telescope, Optics and Precision Engineering 25 (2017) 2614–2619.
[14] R.A. Bernstein, P.J. Mccarthy, K. Raybould, B.C. Bigelow, A.H. Bouchez, J.M. Filgueira, Overview and status of the Giant Magellan Telescope project, SPIE Astronomical Telescopes+ Instrumentation 9145 (2014), 91451C.
[15] S.F. Chen, I. Kao, The Conservative Congruence Transformation for Joint and Cartesian Stiffness Matrices of Robotic Hands and Fingers, The International Journal of Robotics Research 19 (2000) 835–847.
[16] Y. Li, I. Kao, Stiffness control of a three-link redundant planar manipulator using the Conservative Congruence Transformation (CCT), IEEE 3 (2003) 3698–3703.
[17] G. Sommer, Geometric Computing with Clifford Algebras: Theoretical Foundations and Applications in Computer Vision and Robotics, Springer, USA, 2013.
[18] D. Hestenes, New foundations for classical mechanics, Kluwer, USA, 1999.
[19] D. Hildenbrand, Foundations of geometric algebra computing, Springer, USA, 2013.
[20] D. Hestenes, H. Li, A. Rockwood, New Algebraic Tools for Classical Geometry, Geometric Computing with Clifford Algebras, Springer, USA, 2001.
[21] Q. Li, X. Chai, J.N. Xiang, Mobility Analysis of Limited-Degrees-of-Freedom Parallel Mechanisms in the Framework of Geometric Algebra, Journal of Mechanisms & Robotics 8 (2016), 041005(1)-041005(9).
[22] W. Wang, F. Liu, C. Yun, Calibration method of robot base frame using unit quaternion form, Precision Engineering 41 (2015) 47–54.
[23] Z. Huang, Y. Zhao, T. Zhao, Advanced Spatial Mechanism (Chinese Edition), Higher Education Press, China, 2006.
[24] K.H. Hunt, Kinematic geometry of mechanism, Oxford University Press, USA, 1990.
[25] E. Abele, M. Weigold, S. Rothenbucher, Modeling and identification of an industrial robot for machining applications, Ann. CIRP 56 (2007) 387–390.
[26] J. Angeles, On the nature of the Cartesian stiffness matrix, Ingenieria Mecanica Tecnologia Ydesarrollo 3 (2010) 163–170.
[27] F. Wang, Q. An, Y. Fei, Evaluation of the mirror surface figure error based on the SlopeRMS, Optik 127 (2016) 39–42.
[28] X. Liu, X. Tian, Z. Wang, Lightweight design of high volume SiC/Al composite mirror for remote camera, Optik 188 (2019) 64–70.